NANO LETTERS

Letter

pubs.acs.org/NanoLett

Angle-Independent Hot Carrier Generation and Collection Using Transparent Conducting Oxides

Tao Gong and Jeremy N. Munday*

Department of Electrical and Computer Engineering and the Institute for Research in Electronics and Applied Physics, University of Maryland, College Park, Maryland 20742−3511, United States

Supporting Information

ABSTRACT: When high-energy photons are absorbed in a semiconductor or metal, electrons and holes are generated with excess kinetic energy, so-called hot carriers. This extra energy is dissipated, for example, by phonon emission, which results in sample heating. Recovery of hot carriers is important for detectors, sensors, and power convertors; however, the design and implementation of these devices is difficult due to strict requirements on the device geometry, angle of illumination, and incident photon wavelength. Here, we present for the first time a simple, angle-independent device based on transparent conducting electrodes that allows for the generation and collection of hot carriers. We show experimental photocurrent generation from both monochromatic and broadband light sources, show uniform absorption for incident illumination at up to 60° from the surface normal, and find an expected open-circuit voltage in the range 1.5−3.0 V. Under solar illumination, the device is 1 order of magnitude more efficient than previous metal−insulator−metal designs, and power conversion efficiencies >10% are predicted with optimized structures. This approach opens the door to new hot carrier collection devices and detectors based on transparent conducting electrodes.

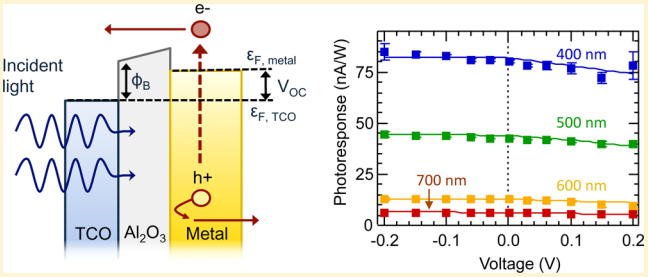

KEYWORDS: *hot carrier, TCO, angular independence, power generation, photodetector, solar energy*

The generation of electrons with sufficiently high kinetic energies, so-called hot electrons, is important to the operation of many semiconductor devices and detectors. For example, Gunn diodes, which display negative differential resistance, operate based on hot electrons generated by strong electric fields.[1] Alternatively, hot carrier generation in photovoltaic applications typically leads to energy loss. High-energy photons create hot carriers within the semiconductor, which relax to the bandgap through the emission of phonons and carrier collisions within pico- to nanoseconds. This carrier cooling (or thermalization) process accounts for a ∼46% loss in the overall efficiency of a photovoltaic device when illuminated by the solar spectrum, reducing the maximum efficiency of a single junction device to ∼33%. Indirect approaches to recovering this loss include the use of multijunction devices[2−4] or semiconducting nanostructures capable of generating multiple carriers from a single photon.[5−9] Although multijunction devices have shown great potential, the direct collection of hot electrons in semiconductor solar cells has proven difficult.[10−12]

Metal−semiconductor (M−S) interfaces have also been explored for hot carrier devices.[13−21] When a metal is illuminated, the electrons in the Fermi gas absorb the incident photons and generate hot electrons with energy higher than the Fermi level. The hot electrons can be injected into the semiconductor, which forms a Schottky junction with the metal, resulting in a Schottky photodetector that is capable of generating current from photons with energy insufficient to generate carriers within the bulk semiconductor. By exploiting localized plasmonic resonances, a silicon−gold device was found to yield an internal quantum efficiency (IQE) of 0.01−0.20% in the near-IR,[13−15] and recently an enhanced photoresponse was found for 1.25 μm illumination using an Au metamaterial absorber on Si.[17] Similarly, in the visible wavelength range (400−700 nm), all-solid-state devices based on TiO_2−Au/Ag nanospheres have been reported to exhibit external quantum efficiency (EQE) of 0.4%−6.0%.[18,20,22] To further elucidate the physical mechanisms involved, a first-principles calculation was recently used to provide a more comprehensive theoretical description of the hot carrier generation process in Ag nanoparticles.[21]

An alternative, semiconductor-free approach can be achieved based on a metal−insulator−metal (M−I−M) structure. Earlier work on M−I−M diodes showed promising results for power conversion and transmission based on the rectification property of these diodes under illumination in the microwave and IR wavelength range.[23,24] Although operation at optical frequencies has proven difficult, low efficiency rectification has been shown by exploiting plasmonic nanogaps.[25] Recently, a hot-carrier-based M−I−M device was proposed by F. Wang et al.

Received: August 24, 2014
Revised: November 23, 2014
Published: December 1, 2014

   dx.doi.org/10.1021/nl503246h | *Nano Lett.* 2015, 15, 147−152

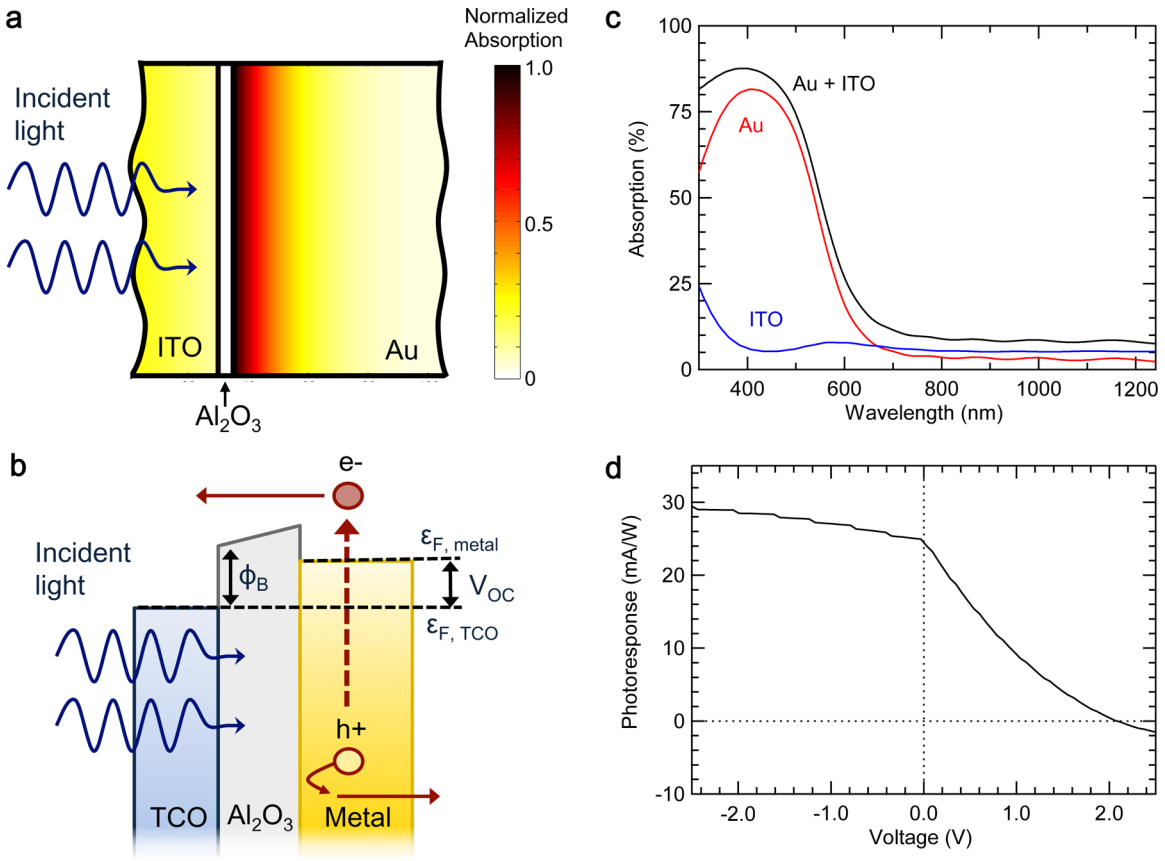

Figure 1. Schematic of the hot carrier device and calculated performance. (a) Cross section of the device under normal incidence illumination. The color scale represents the spatially varying light absorption profile calculated by finite difference time domain simulation under AM 1.5G illumination. (b) Schematic of the hot carrier generation and injection through the insulating barrier while illuminated. (c) Calculated light absorption in the ITO layer, the Au layer, and the total absorption. (d) Calculated photocurrent under AM1.5G illumination and applied bias. The electron density of states is assumed to be parabolic for the calculation.

using a simple Au−Al_2O_3−Au junction.[26] To create anisotropic absorption, a Kretschmann prism coupling configuration was used to couple the incident light into a surface-plasmon-polariton (SPP) mode with the field intensity peaked at the interface between one of the Au films and air. The absorption occurs predominantly in the top Au layer, leading to preferential hot carrier flow from the top Au layer to the bottom one. However, due to this coupling mechanism, SPP modes can only be excited for a particular angle of incidence, which depends on the illumination wavelength. Therefore, for normal incidence illumination, the predicted optimized efficiency is reduced from 2.7% to ∼0.12% under AM 1.5G illumination.

Here, we demonstrate a new hot carrier device based on a transparent conducting oxide (TCO) electrode that enables hot carrier generation and collection independent of incident illumination angle. The device consists of a simple TCO−insulator−metal (TCO−I−M) structure and requires no special coupling mechanism for the incident light. The hot carrier generation yields a wavelength dependent open circuit voltage (in the range of 1.5−3.0 V), and the device can be applied either for power generation or as a photodetector that is almost independent of applied bias voltage within ±0.2 V. Because the TCO's absorption is minimal, ∼80% of the incident light is absorbed in the metal layer and in the vicinity of the oxide interface, leading to highly anisotropic hot carrier flow and predicted power conversion efficiencies >10% under optimal conditions.

Device Fabrication. The device is fabricated by depositing an ITO layer of 30 nm thickness on a BK 7 glass substrate with a stainless-steel shadow mask, which has 4 × 4 aligned horizontal strips of 300 μm width. The sputtering is performed in an AJA sputtering unit at a rate of 70 Å/min with 200 W RF power. The amorphous Al_2O_3 layer is deposited in a Beneq TFS 500 Atomic Layer Deposition (ALD) system at 150 Å/min. 55 operation cycles (resulting in approximately 5 nm of Al_2O_3) are used to ensure accurate and conformal coverage of Al_2O_3 over the underlying surface. The topmost 80 nm gold layer and 2 nm Ti adhesion layer are deposited with another shadow mask with the 4 × 4 vertically aligned strips in a Temescal electron beam deposition system to form a cross junction for the device. Lastly, electrical contact is made to the ITO by attaching a wire to the surface using Chemtronics CW2400 Epoxy A and B mixture. The other contact is realized by directly connecting a probe to the gold electrode.

Experimental Setup. The optical absorption measurement is conducted by using a 6 in. Labsphere integrating sphere and a Thermo Oriel xenon lamp as the light source. The white light from the lamp is separated into different wavelengths with a SPEX 500 M spectrometer. The photocurrent measurement is performed under chopped illumination of a monochromatic collimated beam from a Fianium WhiteLase Supercontinuum laser source. For the electrical measurement, the sample is

dx.doi.org/10.1021/nl503246h | Nano Lett. 2015, 15, 147−152

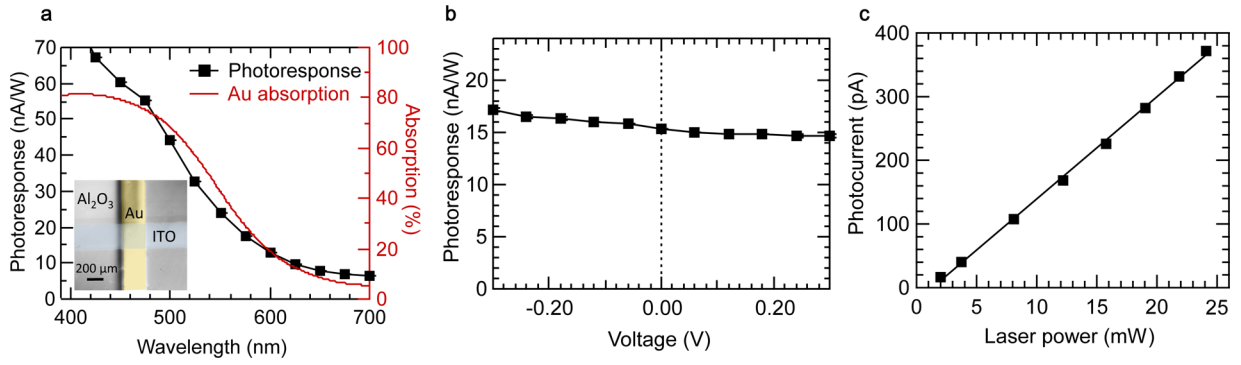

Figure 2. Experimental characterization of the hot carrier device. (a) Photoresponse of the device with respect to the incident wavelength. The photoresponse (left axis) mimics the absorption spectrum (right axis), but the peaks occur at different wavelengths due to the internal carrier emission efficiency, which increases as the wavelengths gets shorter. Inset shows the device cross-junction under 5× optical magnification using a monochrome CCD (false colored for clarity). (b) Photoresponse under biased white light illumination. (c) Photocurrent changes linearly with incident white light power, indicating that the hot carrier generation is a linear process.

connected to a Keithley 2400 SourceMeter, acting as a voltage source and current meter, and to a SR830 DSP lock-in amplifier.

Device Design and Modeling. The performance of a hot carrier device can be determined by considering the following processes: (i) photon absorption, (ii) hot carrier generation, (iii) hot carrier propagation, and (iv) subsequent collection. The detailed modeling for each process[15,26−35] is elaborated in Supporting Information Note 1. Figure 1 shows the predicted performance of a simple planar structure consisting of indium tin oxide (30 nm)−aluminum oxide (5 nm)−gold (80 nm) under illumination. The indium tin oxide (ITO) acts as the transparent conductor and the aluminum oxide (Al_2O_3) is used as the thin insulating barrier to separate ITO and Au. For illumination wavelengths between 300 and 600 nm, absorption predominantly occurs in the Au, leading to a highly anisotropic absorption profile (Figure 1a, c). This exponential decay in the Au promotes electrons in the Fermi gas to higher energy states, simultaneously leaving behind empty hole states. This process leads to preferential hot carrier generation near the Au−Al_2O_3 interface. These hot carriers will subsequently diffuse, during which time they are scattered by the electron gas. The time scale of the electron−electron interaction is ∼500 fs[18,36] for gold; thereafter, these carriers thermally relax producing heat by electron−phonon scattering. Therefore, only a fraction of the carriers find their way to the Au−Al_2O_3 interface. Depending upon the energy and momentum of the carriers that reach the interface, they will either traverse or tunnel through the insulating barrier, ultimately being collected as photocurrent at the ITO electrode (Figure 1b). Because of the preferential absorption in Au, the carriers predominately flow from Au to ITO with a voltage established by the energy barrier between the two electrodes. Thus, for the hot carrier device, the electrodes function as the light absorber, carrier emitter, and carrier collector simultaneously.

Once the absorption is calculated within the device, the optoelectronic response can be determined. The photocurrent−voltage (I−V) characteristic for the device is obtained by the summation of the four current contributions arising from the hot electrons and hot holes from both electrodes (Supporting Information Note 1)

$$I(V) = I_e^{Au-ITO}(V) - I_e^{ITO-Au}(V) - I_h^{Au-ITO}(V) + I_h^{ITO-Au}(V) \quad (1)$$

where the four current components denote the directional hot electron and hole flows (I_e and I_h) between the two electrodes (Au and ITO). The currents depend on the incident spectrum, spatially dependent absorption, bias voltage, electron density of states (EDOS), bandgap of the oxide, barrier height (Φ_B), and the mean-free-paths (MFP) of the carriers. The barrier height at the interface is 0.4 eV for the calculation of optimal performance[26] and the MFPs of Au and ITO are obtained from the literature.[26,27,37−39] Figure 1d shows the calculated I−V response under AM 1.5G solar illumination. For $V < 0$, the photocurrent increases slowly with increasing negative bias, indicating that most of the current comes from hot electrons flowing from the Au to ITO. These electrons have high enough energy to directly traverse the barrier. Alternatively, for $V > 0$, the total current drops faster with increasing bias. In this region, the barrier height seen by the hot electrons in Au is increased and tunneling becomes necessary for those electrons with lower energy ($\Phi_B < \xi < \Phi_B + qV$), thus causing a faster decrease in the current. With larger bias, the current flow becomes negative as reverse electron flow from the ITO to the Au dominates the total current. Meanwhile, the hot electrons generated in Au will find no empty states in ITO to occupy. The contribution to the currents due to the hot holes is also considered; however, their contribution is negligible due to the much larger energy barrier experienced by the hot holes. The overall power conversion efficiency (PCE) is calculated to be 0.95%, which is eight times the value of a planar Au−Al_2O_3−Au junction under normal incidence illumination.[26] For monochromatic illumination at shorter wavelengths, the PCE can reach 3.1% (Supporting Information Table 1), which is comparable to the results of the planar Au−Al_2O_3−Au junction with the Kretchmann SPP prism coupling;[26] however, no special coupling mechanism is necessary for the TCO-based structure.

Another important parameter associated with the I−V characteristic is the fill factor (FF), defined by $FF = (I_{max}V_{max})/(I_{sc}V_{oc})$, where I_{max} and V_{max} are the current and voltage at max power and I_{sc} and V_{oc} are the short circuit current and open circuit voltage, respectively. A larger fill factor corresponds to a more rectangular I−V curve, and hence a higher efficiency device. In our device, the fill factor (Figure 1d) can be improved by modifying the EDOS. To determine the effect of EDOS modification on the device characteristic, two simple models were considered. First, for the above calculations, the EDOS in the metal is assumed to be parabolic,

dx.doi.org/10.1021/nl503246h | Nano Lett. 2015, 15, 147−152

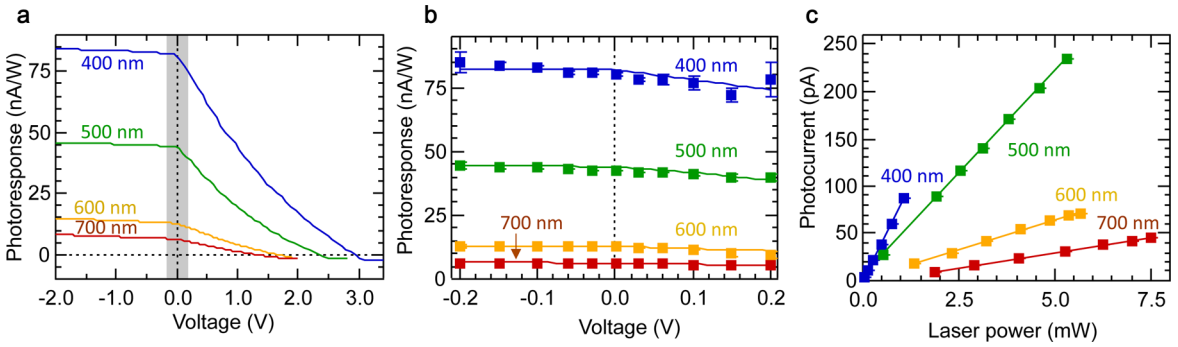

Figure 3. Photoresponse under monochromatic light illumination. (a) Calculated photoresponse showing the V_{oc} increase with incident photon energy, as expected for a hot carrier device. (b) Zoom of the photoresponse−voltage relation (between −0.2 V to +0.2 V, shaded region in (a)) of the device under monochromatic illumination (400, 500, 600, and 700 nm). Markers represent experimental data, while solid lines represent fits from the hot carrier device model. (c) Photocurrent changes linearly with incident power for each illumination wavelength, further confirming the linearity of the hot carrier generation process.

as it would be for a free electron gas. Under this assumption, the generated hot electrons (holes) possess a nearly uniform energy distribution above (below) the Fermi level. Therefore, a large fraction of the hot carriers have an energy lower than the barrier height, which makes traversing the barrier less probable. The efficiency can be further improved if the electrons in the Fermi gas before excitation possess a nonparabolic EDOS. For the second model, we consider the EDOS to have a peak distribution of carriers close to but below the Fermi level, as described below. For most metals, the EDOS is not perfectly parabolic and depends on the crystallography and film thickness. The resulting EDOS may also contain many peaks due to the overlapping bands. For hot carrier generation and collection, the ideal case occurs when most of the electrons in the Fermi gas possess an energy in the vicinity of the Fermi level, ξ_F, before excitation, which is thought to occur in some noble metals.[33] After illumination, almost all excited hot electrons would be distributed in a narrow energy range above the barrier height (Supporting Information Figure 1a). For this case, nearly all hot electrons can traverse the barrier even under positive bias, and the fill factor in the power generation region is significantly improved from 19% to 44% (Supporting Information Figure 1b). In this model, we modify the EDOS by assigning an effective conduction bandedge to be 0.15 eV below the Fermi level.[33] As a result, the PCE improves to 2.33% under AM1.5G solar illumination and reaches 10.7% at short wavelength illumination (Supporting Information Table 2). More substantial EDOS modification may be possible through the utilization of silicide alloys or by exploiting quantum confinement effects in nanoscale materials.[40,41]

Photoresponse under Monochromatic and Broadband Illumination. The photoresponse of the device was experimentally determined over a wavelength range of 400−700 nm and was found to exhibit increased photocurrent for short wavelengths (Figure 2a). The enhanced photoresponse is due to the large absorption at the Au surface relative to the absorption in the ITO. The photoresponse is consistent with the simulated light absorption spectrum, which is also observed in Au−Si photodetectors.[13−15,18] The photoresponse and the absorption differ slightly because the photoresponse depends on both the hot carrier emission/collection and the absorption. Under white light illumination, the hot carrier device is found to generate nearly constant current under both forward and reverse bias (Figure 2b), as expected. Further, hot carrier generation is shown to be a single photon−hot carrier interaction by the linearity of the photocurrent with incident light power for both white light and monochromatic light illumination. (Figures 2c and 3c).

Wavelength-Dependent Hot Carrier Generation and Collection. The $I-V$ characteristic under monochromatic illumination is determined, showing both voltage independent photoresponse for small bias ($|V| < 0.2$ V) and, for larger bias, an open circuit voltage (V_{oc}) that varies with incident photon energy, as expected for an M−I−M hot carrier device (Figure 3a and b). The experimental photoresponse is found to be in good agreement with the model presented here (Figure 3b) throughout the ±0.2 V bias range. Under larger bias, the measurements were unstable due to increased noise and electrical device breakdown. When the theoretical model is extended to higher bias, a wavelength dependent V_{oc} is predicated, which is an order of magnitude larger than previous results, suggesting improved application as a wavelength sensitive hot carrier detector.[42]

The stable photoresponse under bias variation (±0.2 V) shows that this device can also be used in situations where the voltage changes due to (i) variation in potential during operation, (ii) source fluctuations or noise, or (iii) power interruptions. This voltage stability has not been observed in previous M−I−M hot carrier devices.

In order to achieve the idealized photoresponse shown in Figure 1d, several additional considerations need to be made. First, the barrier height $\Phi_B \sim$ 0.4 eV in our simulation is optimized. In reality, the barrier height and the bandgap of the Al_2O_3 film strongly depend on the details of the interface, which may vary significantly with the fabrication methods and surface treatment even for similar interfaces.[26,39] The barrier height extracted from our dark $I-V$ measurements by applying the Fowler-Nordheim model[43] is found to be 20 meV (Supporting Information Figure 3 and Note 2). The much lower barrier height, which probably arises from interface effects such as surface traps, defects, and interface dipoles,[44−46] dramatically increases thermionic emission from the bottom electrode, reducing the overall current and the ultimate efficiency.[26] Second, surface recombination[44,45] at the interface on both sides due to trap states would significantly increase the loss of the carriers, which necessitates the incorporation of loss of carriers in the calculation to fit the experimental data (Figure 3b). Third, the inelastic scattering with the Fermi gas could cause additional energy loss of the hot carriers, allowing fewer of them to reach the interface with sufficient energy.

dx.doi.org/10.1021/nl503246h | Nano Lett. 2015, 15, 147−152

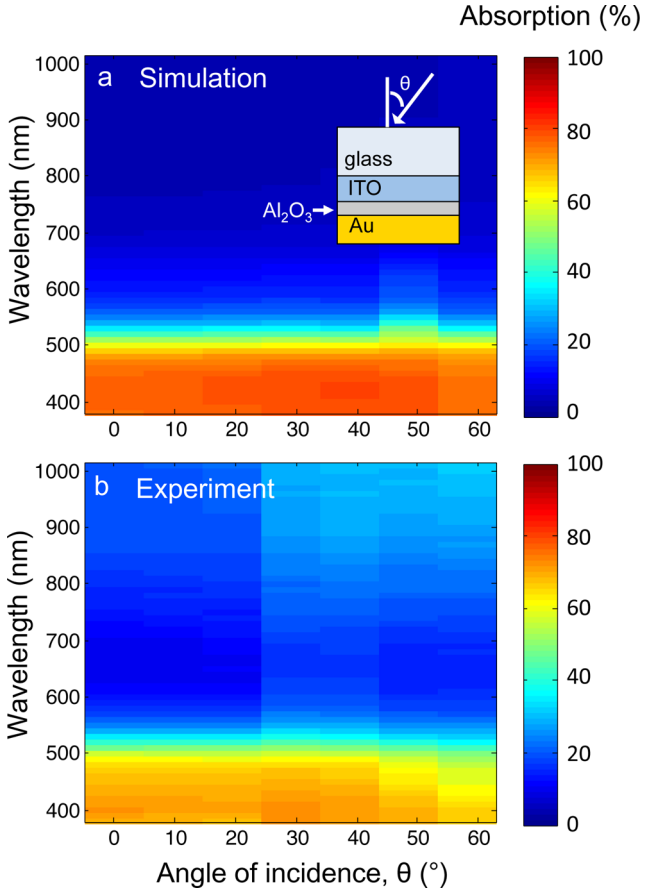

Figure 4. Light absorption spectrum of the device for different incident angles. Simulation (a) and experimental results (b) show a nearly angular-independent absorption of the device, indicating omnidirectional photoresponses. The inset shows a schematic of the device under oblique angle illumination.

Device Dependence on Incident Illumination Angle. The absorption of the device is found to be nearly independent of illumination angle over the entire visible spectrum (Figure 4). This effect is because the absorption mechanism does not rely on surface plasmon coupling, which critically depends on the incident angle of illumination. Instead the absorption is determined by the skin-depth the metal. An integrating sphere setup is used to determine the angular dependence of the absorption for each wavelength. Large absorption occurs at short wavelengths, with Au absorbing most of the light. The broad range angular response shows the device's advantage over structures that require additional coupling mechanisms (e.g., prism coupling), which depend on illumination angle and wavelength. This angular independence is beneficial for solar illumination because light is incident from all angles throughout the course of a day. This device could also be used under concentrated solar light where sunlight is focused with a lens or mirror. Slight differences between the experimental and simulated results (using FDTD) are likely due to differences in the optical properties of the ITO between the experiment and the simulation.

In summary, we have demonstrated hot carrier generation and collection in a simple, planar TCO−insulator−metal configuration. The device has an angle-independent response and is shown to function as a wavelength dependent detector in terms of photocurrent and V_{oc} over the entire visible range. Hot carrier generation and collection is verified experimentally under monochromatic and white light illumination, and the device is shown to operate as a photodetector that is insensitive to applied bias over a range of −0.2 to 0.2 V. As a power conversion device, V_{oc}'s in the range of 1.5−3.0 V are expected. Device simulations are in agreement with experimental results and provide a pathway to power conversion efficiencies >10%.

■ ASSOCIATED CONTENT

Ⓢ Supporting Information

Theoretical modeling of the device, additional figures and tables. This material is available free of charge via the Internet at http://pubs.acs.org.

■ AUTHOR INFORMATION

Corresponding Author

*E-mail: jnmunday@umd.edu.

Author Contributions

J.N.M. and T.G. conceived the idea and device design. T.G. fabricated the devices, performed the calculations, simulations, and experimental measurements. J.N.M. and T.G. wrote the manuscript. J.N.M. supervised the project.

Notes

The authors declare no competing financial interest.

■ ACKNOWLEDGMENTS

This work was supported by the University of Maryland. The authors would like to acknowledge the Maryland Nano-Center and its FabLab for fabrication facilities. The authors also thank J. Murray and D. Ha for technical assistance with absorption measurements.

■ REFERENCES

(1) Sze, S. M. *Physics of Semiconductor Devices*; Wiley-Interscience: Hoboken, NJ, 1981.
(2) Henry, C. Limiting efficiencies of ideal single and multiple energy gap terrestrial solar cells. *J. Appl. Phys.* **1980**, *51*, 4494.
(3) Luque, A.; Hegedus, S. *Handbook of Photovoltaic Science and Engineering*; John Wiley and Sons: Hoboken, NJ, 2011.
(4) Kurtz, S.; Geisz, J. Multijunction solar cells for conversion of concentrated sunlight to electricity. *Opt. Express* **2010**, *18*, A73−A78.
(5) Semonin, O. E.; Luther, J. M.; Choi, S.; Chen, H.-Y.; Gao, J.; Nozik, A. J.; Beard, M. C. Peak External Photocurrent Quantum Efficiency Exceeding 100% via MEG in a Quantum Dot Solar Cell. *Science* **2011**, *334*, 1530−1533.
(6) Blankenship, R. E.; et al. Comparing Photosynthetic and Photovoltaic Efficiencies and Recognizing the Potential for Improvement. *Science* **2011**, *332*, 805−809.
(7) Beard, M. C.; Midgett, A. G.; Hanna, M. C.; Luther, J. M.; Hughes, B. K.; Nozik, A. J. Comparing Multiple Exciton Generation in Quantum Dots To Impact Ionization in Bulk Semiconductors: Implications for Enhancement of Solar Energy Conversion. *Nano Lett.* **2010**, *10*, 3019−3027.
(8) Hanna, M. C.; Nozik, A. J. Solar conversion efficiency of photovoltaic and photoelectrolysis cells with carrier multiplication absorbers. *J. Appl. Phys.* **2006**, *100*, 074510−074518.
(9) McGuire, J. A.; Sykora, M.; Joo, J.; Pietryga, J. M.; Klimov, V. I. Apparent Versus True Carrier Multiplication Yields in Semiconductor Nanocrystals. *Nano Lett.* **2010**, *10*, 2049−2057.
(10) Ross, R. T.; Nozik, A. J. Efficiency of hot-carrier solar energy converters. *J. Appl. Phys.* **1982**, *53*, 3813−3818.
(11) Takeda, Y.; Ito, T.; Motohiro, T.; Konig, D.; Shrestha, S.; Conibeer, G. Hot carrier solar cells operating under practical conditions. *J. Appl. Phys.* **2009**, *105*, 074905.

(12) Tisdale, W. A.; Williams, K. J.; Timp, B. A.; Norris, D. J.; Aydil, E. S.; Zhu, X.-Y. Hot-Electron Transfer from Semiconductor Nanocrystals. *Science* **2010**, *328*, 1543−1547.
(13) Knight, M. W.; Sobhani, H.; Nordlander, P.; Halas, N. Photodetection with Active Optical Antennas. *Science* **2011**, *332*, 702−704.
(14) Knight, M. W.; Wang, Y.; Urban, A. S.; Sobhani, A.; Zheng, B. Y.; Nordlander, P.; Halas, N. J. Embedding Plasmonic Nanostructure Diodes Enhances Hot Electron Emission. *Nano Lett.* **2013**, *13*, 1687−1692.
(15) Sobhani, A.; Knight, M. W.; Wang, Y.; Zheng, B. Y.; King, N. S.; Brown, L. V.; Fang, Z.; Nordlander, P.; Halas, N. J. Narrowband photodetection in the near-infrared with a plasmon-induced hot electron device. *Nat. Commun.* **2013**, *4*, 1643.
(16) Clavero, C. Plasmon-induced hot-electron generation at nanoparticle/metal-oxide interfaces for photovoltaic and photocatalytic devices. *Nat. Photonics* **2014**, *8*, 95−103.
(17) Li, W.; Valentine, J. Metamaterial Perfect Absorber Based Hot Electron Photodetection. *Nano Lett.* **2014**, *14*, 3510−3514.
(18) Reineck, P.; Lee, G. P.; Brick, D.; Karg, M.; Mulvaney, P.; Bach, U. A Solid-State Plasmonic Solar Cell via Metal Nanoparticle Self-Assembly. *Adv. Mater.* **2012**, *24*, 4750−4755.
(19) Nishijima, Y.; Ueno, K.; Yokota, Y.; Murakoshi, K.; Misawa, H. Plasmon-Assisted Photocurrent Generation from Visible to Near-Infrared Wavelength Using a Au-Nanorods/TiO_2 Electrode. *J. Phys. Chem. Lett.* **2010**, *1*, 2031−2036.
(20) Takahashi, Y.; Tatsuma, T. Solid state photovoltaic cells based on localized surface plasmon-induced charge separation. *Appl. Phys. Lett.* **2011**, *99*, 182110.
(21) Manjavacas, A.; Liu, J. G.; KulKarni, V.; Nordlander, P. Plasmon-Induced Hot Carriers in Metallic Nanoparticles. *ACS Nano* **2014**, *8*, 7630−7638.
(22) Tian, Y.; Shi, X.; Lu, C.; Wang, X.; Wang, S. Charge separation in solid-state gold nanoparticles-sensitized photovoltaic cell. *Electrochem. Commun.* **2009**, *11*, 1603−1605.
(23) Grover, S.; Moddel, G. Applicability of Metal/Insulator/Metal (MIM) Diodes to Solar Rectennas. *IEEE J. Photovoltaic* **2011**, *1*, 78−83.
(24) Brown, W. The history of power transmission by radio-waves. *IEEE Trans. Microwave Theory Tech.* **1984**, *32*, 1230−1242.
(25) Ward, D.; Huser, F.; Pauly, F.; Cuevas, J.; Natelson, D. Optical rectification and field enhancement in a plasmonic nanogap. *Nat. Nanotechnol.* **2010**, *5*, 732−736.
(26) Wang, F.; Melosh, N. A. Plasmonic Energy Collection through Hot Carrier Extraction. *Nano Lett.* **2011**, *11*, 5426−5430.
(27) Kovacs, D. A.; Winter, J.; Meyer, S.; Wucher, A.; Diesing, D. Photo and particle induced transport of excited carriers in thin film tunnel junctions. *Phys. Rev. B* **2007**, *76*, 235408.
(28) White, T. P.; Catchpole, K. R. Plasmon-enhanced internal photoemission for photovoltaics: theoretical efficiency limits. *Appl. Phys. Lett.* **2012**, *101*, 073905.
(29) Berglund, C. N.; Spicer, W. E. Photoemission studies of copper and silver: theory. *Phys. Rev.* **1964**, *136*, A1030−A1044.
(30) Scales, C.; Berini, P. Thin-Film Schottky Barrier Photodetector Models. *IEEE J. Quantum Electron.* **2010**, *46*, 633−643.
(31) Shepard, K. W. Photocurrents through thin films of Al_2O_3. *J. Appl. Phys.* **1965**, *36*, 796−799.
(32) Jennison, D. R.; Schultz, P. A.; Sullivan, J. P. Evidence for interstitial hydrogen as the dominant electronic defect in nanometer alumina films. *Phys. Rev. B* **2004**, *69*, 041405.
(33) Chan, E. Y.; Card, H. C.; Teich, M. C. Internal photoemission mechanisms at interfaces between germanium and thin metal films. *IEEE J. Quantum Electron.* **1980**, *16*, 373−381.
(34) Braunstein, A. I.; Braunstein, M.; Picus, G. S. Hot-electron attenuation in thin Al_2O_3 films. *Phys. Rev. Lett.* **1965**, *15*, 956−958.
(35) Simmons, J. G. Generalized formula for electric tunnel effect between similar electrodes separated by a thin insulating film. *J. Appl. Phys.* **1963**, *34*, 1793−1803.
(36) Voisin, C.; Del Fatti, N.; Christofilos, D.; Vallee, F. Ultrafast electron dynamics and optical nonlinearities in metal nanoparticles. *J. Phys. Chem. B* **2001**, *105*, 2264−2280.
(37) Pammi, S. V.; Chanda, A.; Ahn, J.-K.; Park, J.-H.; Cho, C.-R.; Lee, W.-J.; Yoon, S.-G. Low Resistivity ITO Thin Films Deposited by NCD Technique at Low Temperature: Variation of Tin Concentration. *J. Electrochem. Soc.* **2010**, *157*, H937−H941.
(38) Bellingham, J.; Phillips, W.; Adkins, C. Electrical and optical-properties of amorphous indium oxide. *J. Phys.: Condens. Matter* **1990**, *2*, 6207−6221.
(39) Chalabi, H.; Schoen, D.; Brongersma, M. L. Hot-Electron Photodetection with a Plasmonic Nanostripe Antenna. *Nano Lett.* **2014**, *14*, 1374−1380.
(40) Slepko, A.; Demkov, A. Band engineering in silicide alloys. *Phys. Rev. B* **2012**, *85*, 035311.
(41) Kamat, P. Quantum Dot Solar Cells. Semiconductor Nanocrystals as Light Harvesters. *J. Phys. Chem. C* **2008**, *112*, 18737−18753.
(42) Wang, F.; Melosh, N. A. Power-independent wavelength determination by hot carrier collection in metal-insulatormetal devices. *Nat. Commun.* **2013**, *4*, 1711.
(43) Cowell, E. W., III; Muir, S. W.; Keszler, D. A.; Wager, J. F. Barrier height estimation of asymmetric metal-insulator-metal tunneling diodes. *J. Appl. Phys.* **2013**, *114*, 213703.
(44) Skarlatos, Y.; Barker, R.; Yelon, A. Traps in Al_2O_3 detected by tunneling. *J. Appl. Phys.* **1976**, *47*, 4593−4597.
(45) Ealet, B.; Elyakhloufi, M.; Gillet, E.; Ricci, M. Electronic and crystallographic structure of gamma-alumina thin-films. *Thin Solid Films* **1994**, *250*, 92−100.
(46) Tung, R. T. The physics and chemistry of the Schottky barrier height. *Appl. Phys. Rev.* **2014**, *1*, 011304.